Modelling of gas-sensitive conducting polymer devices

J.W. Gardner
P.N. Bartlett
K.F.E. Pratt

Indexing terms: Conducting polymers, Gas-sensitive polymers, Gas sensor, Polymer films

Abstract: Recent studies have shown that conducting polymers are sensitive to a wide range of gases and vapours and may be used in gas-sensing microelectronic devices. The authors present a basic model for polymer gas sensors which consists of a thin uniform polymer film lying on top of a pair of either semi-infinite or finite coplanar electrodes supported by an insulating substrate. It is assumed that the gas, or vapour, diffuses into the film and is, simultaneously, adsorbed at sites randomly distributed throughout the film. The diffusion and adsorption equations are presented in terms of several fundamental dimensionless parameters which describe the underlying chemical and physical properties of the system. Numerical solutions to the equations are calculated for both the gas and adsorbate profiles within the films at various times. These numerical solutions are compared with approximate analytical expressions previously derived for diffusion-rate limited, reaction-rate limited and intermediate cases, and show good agreement. Finally, a semiconductor model of electronic conduction in gas-sensitive polymer films is developed to calculate the theoretical device response to the sorption of organic vapours. This model can be used to investigate the effects of device geometry on sensor response and is therefore a useful design tool for evaluating novel device structures. The model may also be extended to cover other types of device, such as capacitive or mass balance.

1 Introduction

It is well established that the electrical conductivity of conducting polymers, such as poly(pyrrole), is affected by exposure to various organic and inorganic gases and this has led to the investigation, by a number of groups, of these materials as gas sensors. Early studies concentrated on the use of poly(pyrrole), formed either chemically [1] or by electrochemical polymerisation [2, 3], to detect ammonia and other inorganic gases, such as NO_2 and H_2S [2, 4]. Subsequently it was found that a wide range of organic vapours also affected the conductivities of these materials and that they could be used in microelectronic devices [5–10]. The observation that these materials were sensitive to a range of gases has led to their use in sensor arrays responsive to complex mixtures [11–14].

Conducting polymers are attractive materials for gas sensor applications because a wide range of such polymers are already known [15–17] and because new polymers can be designed and synthesised by the substitution of different functional groups onto the polymer backbone. In addition, the materials respond to vapours at room temperature [9] and can be deposited onto microelectronic structures under controlled conditions by electrochemical polymerisation across the gap between two microband electrodes [2, 18].

Despite this interest in the potential applications of these materials as gas sensors, the mechanism of the interaction between the polymer and the gas molecules, and the manner in which this generates a change in the properties of the polymer, remain the subject of debate. Several possible modes of interaction can be envisaged including swelling of the polymer, interaction between the gas molecules and charge carriers on the polymer chain, interaction between the gas molecules and the counter ions within the polymer and oxidation or reduction of the polymer by the gas [13]. Studies in the literature suggest that one or more of these mechanisms may be operative depending on the particular combination of polymer and gas considered.

The only organic vapour system which has been studied in any detail is the interaction of methanol with poly(pyrrole). Studies by Bartlett and Ling-Chung showed that for poly(pyrrole)/tetrafluoroborate the conductivity changes on exposure to methanol were consistent with a simple binding isotherm and that there was no evidence for diffusion limitation [9, 10]. Based on work function and optical absorption measurements Blackwood and Josowicz, using poly(pyrrole)/tosylate and poly(pyrrole)/tetrafluoroborate, suggested that there was electron transfer between the methanol molecules and the polymer to produce a charge-transfer complex [19]. Subsequent measurements of changes in work function, mass and optical absorption, again for poly(pyrrole)/tosylate and tetrafluoroborate, were taken to support this view; although at high concentrations of methanol vapour it was noted that there were also plasticisation effects [20, 21]. The effect of the different counter ions was accounted for by differences in the partition of the methanol into the two films. Using results from mass and conductivity measurements for

Paper 2170G (E3), first received 13th October 1994 and in revised form 12th June 1995

J.W. Gardner is with the Centre of Nanotechnology & Microengineering, Department of Engineering, University of Warwick, Coventry CV4 7AL, United Kingdom

P.N. Bartlett and K.F.E. Pratt are with the Department of Chemistry, University of Southampton, Southampton SO17 1BJ, United Kingdom

poly(pyrrole)/bromide, Slater *et al.* [22] have concluded that the swelling of the polymer by the methanol vapour is the dominant effect and that this causes a change in the polymer from a glass-like to a rubber-like state which affects its conducting behaviour. In comparing the results from different authors it is important to remember that the properties and morphology of these films can be changed significantly by changes in the deposition conditions and counter ion employed.

In this paper, we consider a very simple model for the coupled diffusion of gas species into, and interaction with, fixed sites within a polymer film. We compare the results for our previous semi-analytical treatment of this problem [23] with the results of finite difference simulation of the problem and we examine the conductivity changes that such a model predicts for devices with various electrode geometries.

2 Diffusion reaction model

The general problem of interest here consists of a gaseous species, A, diffusing into a homogeneous polymer film of thickness, L, deposited across the gap between two thin electrodes on an impermeable substrate (see Fig. 1). We

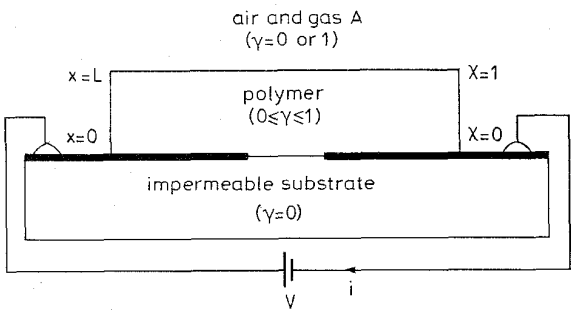

Fig. 1 *Geometrical structure of a planar polymeric device for sensing organic vapours with dimensionless parameters defined*

assume that the polymer contains a uniform distribution, N, of immobile adsorption sites, ⟨site⟩. For simplicity we assume that the adsorption process is described by the Langmuir adsorption isotherm, i.e.

$$A + \langle \text{site} \rangle \underset{k_b}{\overset{k_f}{\Leftrightarrow}} \langle A \rangle \tag{1}$$

where k_f and k_b are the forward and backward reaction rates, respectively. Exploiting the geometry of a planar film allows the use of a one-dimensional model in which the sorbate concentration, a, and site occupancy, θ, profiles are only a function of the distance x and time t.

The overall process can now be described by a modified diffusion equation in dimensionless form,

$$\frac{\partial^2 \gamma}{\partial \chi^2} - \frac{\partial \gamma}{\partial \tau} = \frac{\eta}{\lambda} \frac{\partial \theta}{\partial \tau} \tag{2}$$

where χ is the dimensionless distance parameter (x/L), τ is the dimensionless time parameter (Dt/L^2), γ the normalised gas concentration (a/a_∞) and a_∞ is the external gas concentration. η and λ are dimensionless parameters given by KN and Ka_∞, respectively, and thus depend upon material properties such as the equilibrium constant K (k_f/k_b) and the density of sites N. The gas that is bound (or released on desorption) from the diffusion process by sites can be related to the sorption kinetics by,

$$\eta \frac{\partial \theta}{\partial \tau} = \kappa \lambda \gamma (1 - \theta) - \kappa \theta \tag{3}$$

where κ is a dimensionless parameter that equals the ratio of forward reaction-rate to diffusion-rate, $k_f NL^2/D$. Eqns. 2 and 3 may now be solved with suitable boundary conditions to obtain the adsorption and desorption concentration, $\gamma(\chi, \tau)$, and site occupancy $\theta(\chi, \tau)$ profiles.

3 Analytical solutions to sorbate profiles

No exact analytical solution to the coupled nonlinear partial differential eqns. 2 and 3 has yet been found but approximate analytical solutions have been derived by us for the six limiting cases [23, 24]. Fig. 2 shows the case

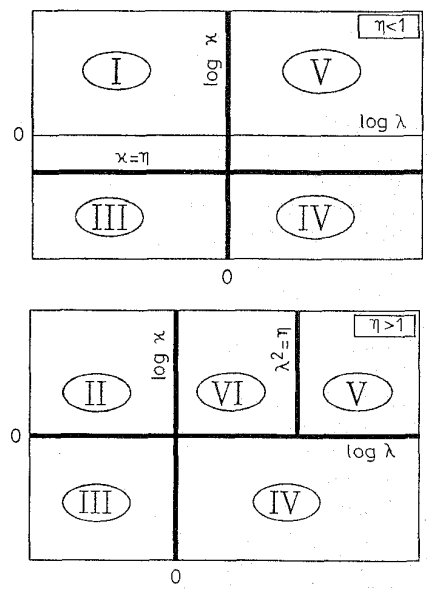

Fig. 2 *Case diagram showing different solutions to the diffusion reaction problem*

I–pure diffusion; II–slow diffusion; III–unsaturated (linear) reaction kinetics; IV–saturated reaction kinetics; V–saturated (nonlinear) reaction kinetics; VI–mixed diffusion reaction process

diagram that contains the full solution space defined by the three dimensionless parameters (κ, λ, η) with the six limiting cases I to VI marked on it. In case I ($\lambda < 1$, $\eta < 1$, $\kappa > \eta$) we have a pure diffusion process because the diffusion rate is much slower than the reaction rate *and* there are few adsorption sites to modify the diffusion process. In case II ($\lambda < 1$, $\eta > 1$, $\kappa > 1$) there are now a significant number of reaction sites available to adsorb the diffusing gas and slow the diffusion process down by a factor of $\sim 1/\eta$ [25].

Cases III and IV relate to the converse situation in which the diffusion rate is much faster than the reaction rate. Case III ($\lambda < 1$, $\kappa < 1$, $\kappa < \eta$) occurs when the reaction kinetics are in the linear (unsaturated) region of the isotherm (i.e. $\theta \ll 1$) whereas case IV ($\lambda > 1$, $\kappa < 1$, $\kappa < \eta$) describes the saturated region of the isotherm ($\theta \approx 1$). Case V ($\lambda > 1$, $\lambda^2 > \eta$, $\kappa > 1$, $\kappa > \eta$) describes the saturated region of the isotherm when the kinetics are fast so that equilibrium is maintained between free and bound species. Finally, case VI ($\lambda > 1$, $\lambda^2 < \eta$, $\eta > 1$, $\kappa > 1$) represents the situation between cases II and V in which neither the reaction process nor the diffusion process dominates; this is commonly referred to as the 'moving boundary problem' [26]. In case VI a boundary between the saturated and unsaturated regions of the film propagates inwards (or outwards). Table 1 gives the expressions for the approximate analytical solutions to all of these six cases which have been derived elsewhere [23].

Table 1: Approximate analytical expressions for the gas concentration and site occupancy sorption profiles in conducting polymer films

Adsorption profiles	Desorption profiles
Case I: ($\lambda < 1$, $\eta < 1$, $\kappa > \eta$)	
$\gamma(\chi, \tau) = 1 - \frac{2}{\pi}\sum_{n=0}^{\infty} \frac{\cos[(n+1/2)\pi\chi] \exp[-(n+1/2)^2\pi^2\tau]}{(-1)^n(n+1/2)}$	$\gamma(\chi, \tau) = \frac{2}{\pi}\sum_{n=0}^{\infty} \frac{\cos[(n+1/2)\pi\chi] \exp[-(n+1/2)^2\pi^2\tau]}{(-1)^n(n+1/2)}$
$\theta(\chi, \tau) = \lambda\gamma$	$\theta(\chi, \tau) = \lambda\gamma$
Case II: ($\lambda < 1$, $\eta > 1$, $\kappa > 1$)	
$\gamma(\chi, \tau) = 1 - \frac{2}{\pi}\sum_{n=0}^{\infty} \frac{\cos[(n+1/2)\pi\chi] \exp[-(n+1/2)^2\pi^2\tau/\eta]}{(-1)^n(n+1/2)}$	$\gamma(\chi, \tau) = \frac{2}{\pi}\sum_{n=0}^{\infty} \frac{\cos[(n+1/2)\pi\chi] \exp[-(n+1/2)^2\pi^2\tau/\eta]}{(-1)^n(n+1/2)}$
$\theta(\chi, \tau) = \lambda\gamma$	$\theta(\chi, \tau) = \lambda\gamma$
Case III: ($\lambda < 1$, $\kappa < 1$, $\kappa < \eta$)	
$\gamma(\chi, \tau) = 1 - \frac{2}{\pi}\sum_{n=0}^{\infty} \frac{\cos[(n+1/2)\pi\chi] \exp[-(n+1/2)^2\pi^2\tau]}{(-1)^n(n+1/2)}$	$\gamma(\chi, \tau) = \frac{2}{\pi}\sum_{n=0}^{\infty} \frac{\cos[(n+1/2)\pi\chi] \exp[-(n+1/2)^2\pi^2\tau]}{(-1)^n(n+1/2)}$
$\theta(\chi, \tau) = \lambda[1 - \exp(-\kappa\tau/\eta)]$	$\theta(\chi, \tau) = 1 - \lambda[1 - \exp(-\kappa\tau/\eta)]$
Case IV: ($\kappa < 1$, $\kappa < \eta$, $\lambda > 1$)	
$\gamma(\chi, \tau) = 1 - \frac{2}{\pi}\sum_{n=0}^{\infty} \frac{\cos[(n+1/2)\pi\chi] \exp[-(n+1/2)^2\pi^2\tau]}{(-1)^n(n+1/2)}$	$\gamma(\chi, \tau) = \frac{2}{\pi}\sum_{n=0}^{\infty} \frac{\cos[(n+1/2)\pi\chi] \exp[-(n+1/2)^2\pi^2\tau]}{(-1)^n(n+1/2)}$
$\theta(\chi, \tau) = 1 - \exp(-\lambda\gamma\kappa\tau/\eta)$	$\theta(\chi, \tau) = \exp(-\kappa(\tau - \tau_d)/\eta)/(1 + \exp(-\kappa(\tau - \tau_d)/\eta))$ with $\tau_d = [4\ln(4\lambda/\pi)]/\pi^2$
Case V: ($\kappa > 1$, $\kappa > \eta$, $\lambda > 1$, $\lambda^2 > \eta$)	
$\gamma(\chi, \tau) = 1 - \frac{2}{\pi}\sum_{n=0}^{\infty} \frac{\cos[(n+1/2)\pi\chi] \exp[-(n+1/2)^2\pi^2\tau]}{(-1)^n(n+1/2)}$	$\gamma(\chi, \tau) = \frac{2}{\pi}\sum_{n=0}^{\infty} \frac{\cos[(n+1/2)\pi\chi] \exp[-(n+1/2)^2\pi^2\tau]}{(-1)^n(n+1/2)}$
$\theta(\chi, \tau) = \lambda\gamma/(1 + \lambda\gamma)$	$\theta(\chi, \tau) = \lambda\gamma/(1 + \lambda\gamma)$
Case VI: ($\kappa > 1$, $1 < \lambda^2 < \eta$, $\eta > 1$)	
For $\tau < \tau_*$ where $\tau_* = 0.59\eta/\lambda$	
$\gamma_1(\chi < \chi_*, \tau) \approx \frac{\gamma_*}{\text{erfc}(\zeta\eta^{1/2})}\text{erfc}\left[\frac{\eta^{1/2}(1-\chi)}{2\tau^{1/2}}\right] + \varepsilon(\chi, \tau)$	$\gamma(\chi, \tau) \approx \frac{2}{\pi}\sum_{n=0}^{n=\infty} \frac{\cos[(n+1/2)\pi\chi] \exp[-(n+1/2)^2\pi^2\zeta/\eta]}{(-1)^n(n+1/2)}$
$\gamma_2(\chi > \chi_*, \tau) \approx 1 - \frac{1-\gamma_*}{\text{erf}\,\zeta}\text{erf}\left[\frac{(1-\chi)}{2\tau^{1/2}}\right] + \varepsilon(\chi, \tau)$	where,
where $\gamma_* = 1 - 2\zeta\tau^{1/2}$ and $\varepsilon(\chi, \tau) \approx \text{erfc}\left[\frac{\eta^{1/2}(1+\chi)}{2\tau^{1/2}}\right] - \text{erfc}\left[\frac{\eta^{1/2}(3-\chi)}{2\tau^{1/2}}\right]$	$\zeta = \tau + 2\lambda\int_{\tau'=0}^{\tau'=\tau}\text{erf}\left[\frac{\eta^{1/2}}{2(1+\lambda)\tau'^{1/2}}\right]d\tau' + \lambda^2\int_{\tau'=0}^{\tau'=\tau}\text{erf}^2\left[\frac{\eta^{1/2}}{2(1+\lambda)\tau'^{1/2}}\right]d\tau'$
and the value of ζ is the root of $\frac{\exp(-\zeta^2)}{\text{erf}(\zeta)} - \frac{\gamma_*\exp(-\zeta^2\eta)}{\eta^{1/2}(1-\gamma_*)\text{erfc}(\zeta\eta^{1/2})} = \frac{\eta\pi^{1/2}\zeta}{\lambda(1-\gamma_*)}$	
For $\tau > \tau_*$	
$\gamma(\chi, \tau) = 1 + \frac{2}{\pi}\sum_{n=1}^{n=\infty}\frac{1}{n}[\cos(n\pi) - 1]\sin[\tfrac{1}{2}n\pi(\chi+1)]\exp[-n^2\pi^2(\tau-\tau_*)/4]$ $+ 2\sum_{n=1}^{n=\infty}\sin[\tfrac{1}{2}n\pi(\chi+1)]\exp[-n^2\pi^2(\tau-\tau_*)/4]\int_{\chi'=0}^{\chi'=1}\gamma_2(\chi', \tau_*)\sin[\tfrac{1}{2}n\pi(\chi'+1)]\,d\chi'$	
$\theta(\chi, \tau) = \lambda\gamma/(1 + \lambda\gamma)$	$\theta(\chi, \tau) = \lambda\gamma/(1 + \lambda\gamma)$

We will now compare the solutions calculated from these approximate analytical equations with exact numerical solutions of the full diffusion reaction equations.

4 Comparison between numerical and analytical concentration profiles

4.1 Numerical method

Digital simulations of the model were performed using a finite difference method, which has been previously described in detail by Britz [27]. Only the important changes in the technique will be described here. Initially, the explicit point method was used, with linear point spacing. Diffusion of the gas A was modelled by the usual finite difference form of Fick's second law. The concentration of the gas at the inner boundary was determined by the 5 point flux approximation [27], while setting the flux through the inner boundary to zero. The sorption kinetics (rates k_f and k_b) were considered as two separate reactions rather than an equilibrium because we are concerned here with the transient responses. Kinetics were calculated after mass transport as described [27].

The explicit method was found to give good agreement with the approximate analytical solutions in the limiting cases, but required considerable computational time when solving for very slow reaction kinetics. The latter also requires a large number of iterations (of the order of one million or more) for equilibrium to be achieved, which can cause an accumulation of significant rounding errors. To overcome this problem, a more implicit simulation can be used, such as that of Crank and Nicolson [28]. This allows large diffusion terms to be analysed. One drawback of the Crank–Nicolson method is that reaction kinetics of higher order than one can only be applied if simplifying approximations are used [27]. The complexity of applying the Crank–Nicolson method to all six diffusion reaction cases was not necessary as the method is only required when slow reaction kinetics occurs. The Crank–Nicholson method was therefore used to model diffusion, while reaction kinetics were dealt with explicitly as stated above. This allowed the numerical simulation time to be reduced by a factor of 100 in some cases. For simulations with fast reaction kinetics, where the value of the model diffusion coefficient [27] is less than 0.45, the explicit method was used, as it required less processor time than Crank–Nicolson for the same accuracy. Typical numerical simulation times ranged from less than 1 minute to 5 hours

using a personal computer (33 MHz, 80486 DX processor). In contrast all approximate expressions calculated the solution in under a second. The program was written using Borland Turbo Pascal. The source code is available from the authors on request.

4.2 Results for Cases I to VI

Table 2 gives the values of the dimensionless parameters used to verify the accuracy of the approximate analytical expressions for the gas concentration $\gamma(\chi, \tau)$ and site occupancy $\theta(\chi, \tau)$ profiles. The values were chosen to provide one typical example from each region of the cases. Values close to case boundaries have also been analysed elsewhere to check the continuity of the approximate solutions. In the ideal adsorption process, all polymer sites are initially empty ($\theta = 0$, $\tau = 0$) and the external gas concentration is a step function ($\gamma = 0$ for $\tau < 0$ and $\gamma = 1$ for $\tau \geqslant 0$). The ideal desorption process starts with the gas concentration and site occupancy at equilibrium ($\gamma = 1$ and $\theta = \theta_\infty$ at $\tau = 0$) followed by a step change in the external gas concentration to zero at $\tau \geqslant 0$).

Figs. 3 to 26 show results of the numerical solution for each case together with the approximate analytical solutions calculated from the expressions given in Table 1 and the values given in Table 2. The adsorption and desorption profiles for Cases I and II (Figs. 3–10) are symmetrical because the process is diffusion rate limited.

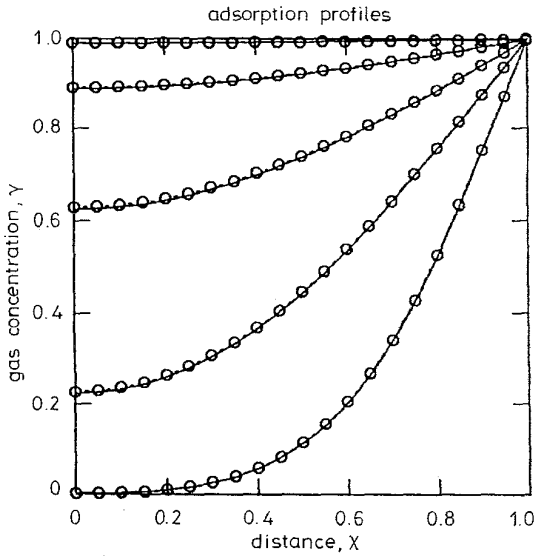

Fig. 3 *Case I adsorption profiles for gas concentration*

The solid lines show the numerical solution and the symbols show the approximate analytical solution with $\kappa = 1$, $\lambda = 0.01$ and $\eta = 0.01$. (See Table 2 for values of τ)

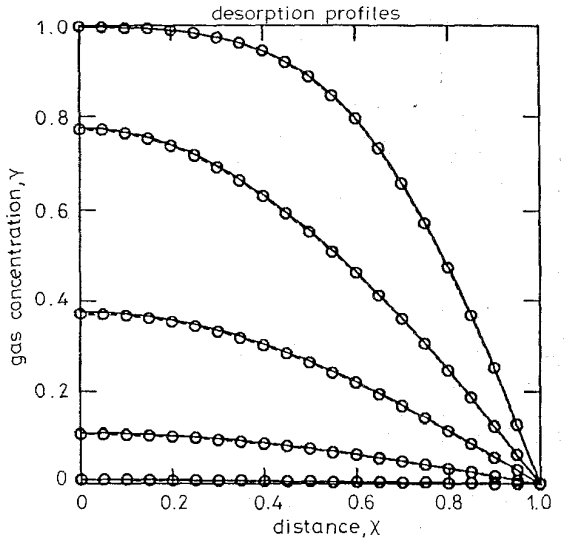

Fig. 4 *Case I desorption profiles for gas concentration*

The solid lines show the numerical solution and the symbols show the approximate analytical solution with $\kappa = 1$, $\lambda = 0.01$ and $\eta = 0.01$. (See Table 2 for values of τ)

Figs. 11–14 show the case for pure kinetics (linear region) in which the gas diffuses through very rapidly and so the site occupancy is symmetric and independent of distance. Figs. 15–18 show Case IV in which the sites are saturated and so the profiles are asymmetric with the desorption process being much slower. Figs. 19–22 show Case V in which the reaction kinetics are in the nonlinear region. Clearly, the adsorption and desorption profiles are dissimilar with the desorption process being once again much slower. In the region of $\eta > 1$, the profiles in Cases IV and V look similar but the larger τ values meant that the numerical solution for desorption could not be calculated in a reasonable time.

Finally, in Case VI (Figs. 23–26) it is possible to see the boundary between filled and empty sites moving into the film on adsorption and again a much slower desorption process. When one considers the wide range of physical and chemical properties covered by the model (6 or 7 decades) then a reasonable agreement is achieved in all cases between our approximate analytical solution

Table 2: Values of parameters used to calculate the typical gas concentration and site occupancy profiles for sorption process

Fig. No.	Case	Description	κ	λ	η	τ (Adsorb/desorb)
3	I	Pure diffusion	1	0.01	0.01	0.05, 0.2, 0.5, 1.0, 2.0 0.05, 0.2, 0.5, 1.0, 2.0
4	II	Slow diffusion	100	0.01	1000	100, 250, 500, 1000, 2000 500, 1000, 2000, 5000, 10000
5	III	Unsaturated (linear) reaction	10^{-4}	0.01	0.01	35, 70, 150, 300, 600 35, 70, 150, 300, 600
—	III	Unsaturated (linear) reaction[a]	0.01	0.01	1000	—
6	IV	Saturated reaction	10^{-4}	100	0.01	0.3, 0.75, 1.5, 3.0, 6.0 10, 50, 100, 300, 600
—	IV	Saturated reaction[a]	0.01	100	1000	—
7	V	Saturated (nonliner) reaction	1	100	0.01	0.01, 0.02, 0.04, 0.08, 0.16, 0.32 0.05, 0.2, 0.5, 1.0, 2.0, 5.0
—	V	Saturated (nonlinear) reaction[a]	100	1000	1000	—
8	VI	Hybrid process	100	10	1000	2, 10, 50, 100, 200 10, 200, 500, 1000, 2000

[a] Profiles not plotted as desorption process too ill-conditioned to solve numerically.

Values for $\eta > 1$ have been calculated for adsorption using the simulation but desorption takes an impractical length of time. However, profiles are similar to $\eta < 1$.

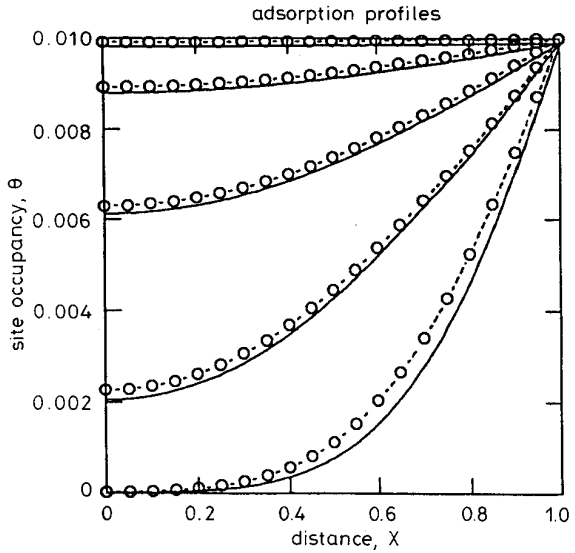

Fig. 5 *Case I adsorption profiles for site occupancy*

The solid lines show the numerical solution and the symbols show the approximate analytical solution with $\kappa = 1$, $\lambda = 0.01$ and $\eta = 0.01$. (See Table 2 for values of τ)

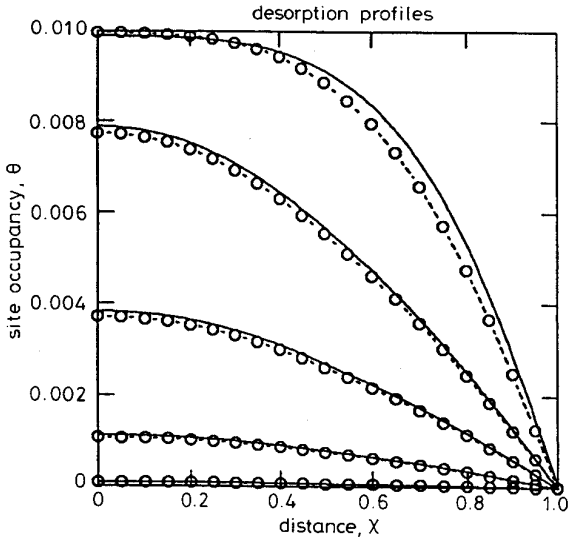

Fig. 6 *Case I desorption profiles for site occupancy*

The solid lines show the numerical solution and the symbols show the approximate analytical solution with $\kappa = 1$, $\lambda = 0.01$ and $\eta = 0.01$. (See Table 2 for values of τ)

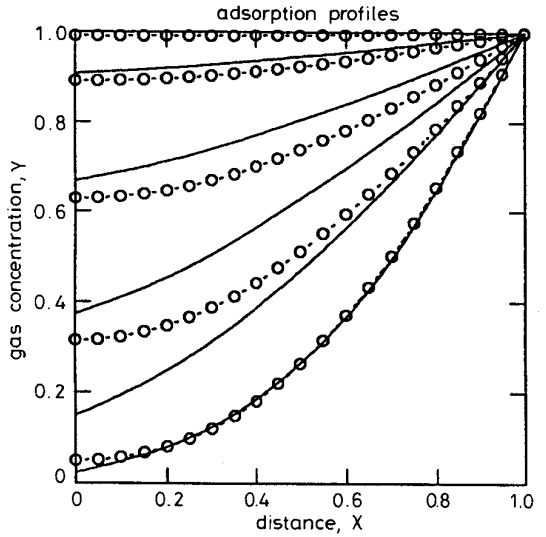

Fig. 7 *Case II adsorption profiles for gas concentration*

The solid lines show the numerical solution and the symbols show the approximate analytical solution with $\kappa = 100$, $\lambda = 0.01$ and $\eta = 1{,}000$. (See Table 2 for values of τ)

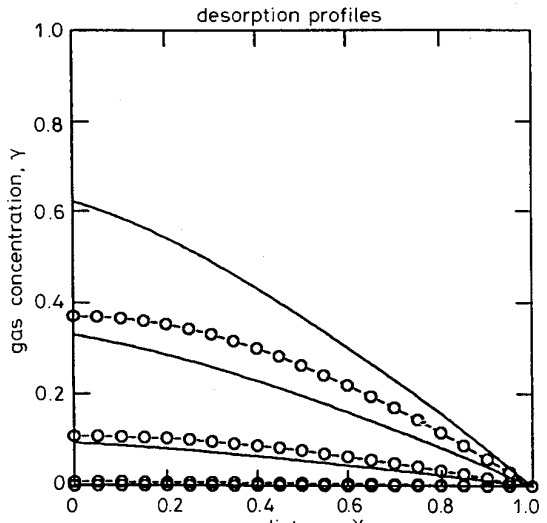

Fig. 8 *Case II desorption profiles for gas concentration*

The solid lines show the numerical solution and the symbols show the approximate analytical solution with $\kappa = 100$, $\lambda = 0.01$ and $\eta = 1{,}000$. (See Table 2 for values of τ)

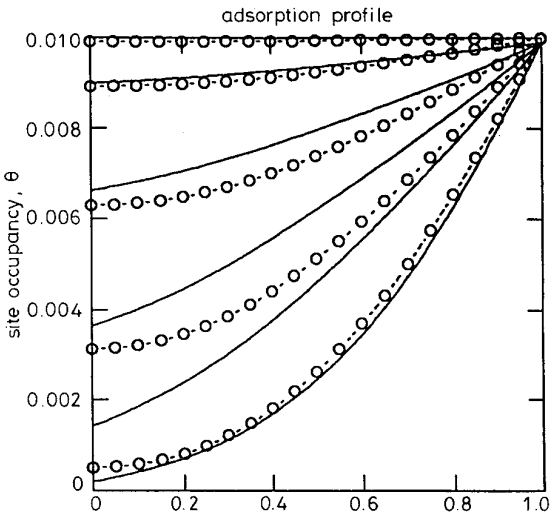

Fig. 9 *Case II adsorption profiles for site occupancy*

The solid lines show the numerical solution and the symbols show the approximate analytical solution with $\kappa = 100$, $\lambda = 0.01$ and $\eta = 1{,}000$. (See Table 2 for values of τ)

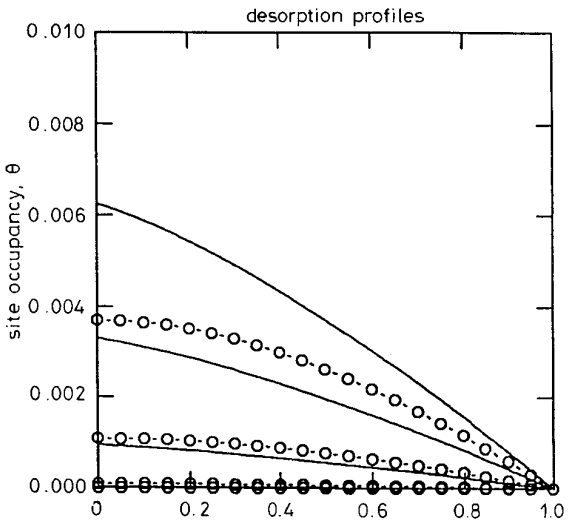

Fig. 10 *Case II desorption profiles for site occupancy*

The solid lines show the numerical solution and the symbols show the approximate analytical solution with $\kappa = 100$, $\lambda = 0.01$ and $\eta = 1{,}000$. (See Table 2 for values of τ)

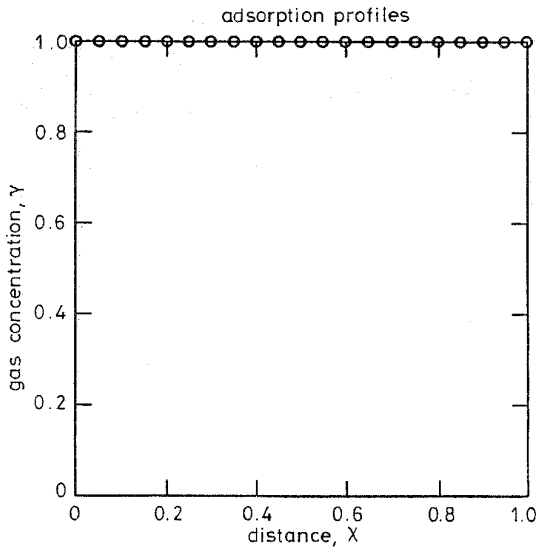

Fig. 11 *Case III adsorption profiles for gas concentration*

The solid lines show the numerical solution and the symbols show the approximate analytical solution with $\kappa = 10^{-4}$, $\lambda = 0.01$ and $\eta = 0.01$. (See Table 2 for values of τ)

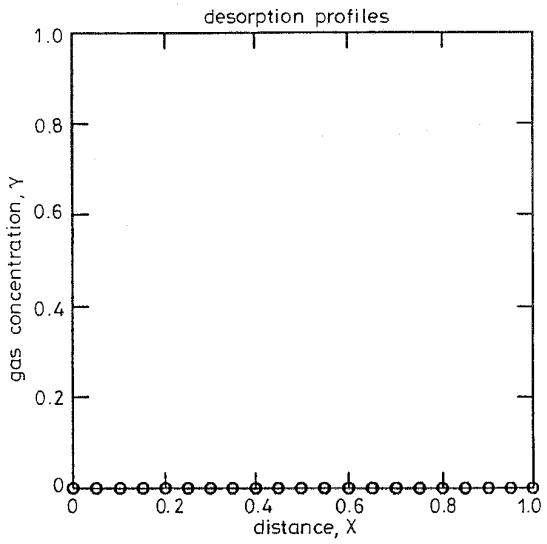

Fig. 12 *Case III desorption profiles for gas concentration*

The solid lines show the numerical solution and the symbols show the approximate analytical solution with $\kappa = 10^{-4}$, $\lambda = 0.01$ and $\eta = 0.01$. (See Table 2 for values of τ)

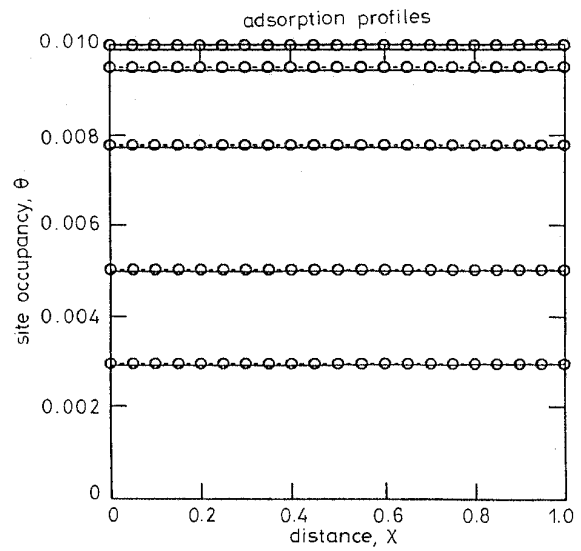

Fig. 13 *Case III adsorption profiles for site occupancy*

The solid lines show the numerical solution and the symbols show the approximate analytical solution with $\kappa = 10^{-4}$, $\lambda = 0.01$ and $\eta = 0.01$. (See Table 2 for values of τ)

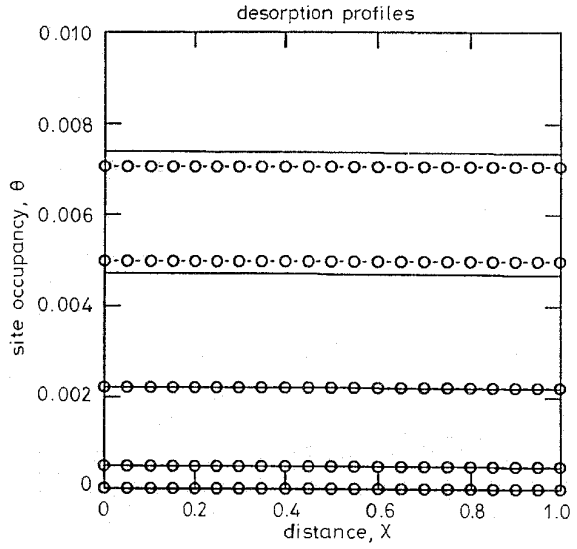

Fig. 14 *Case III desorption profiles for site occupancy*

The solid lines show the numerical solution and the symbols show the approximate analytical solution with $\kappa = 10^{-4}$, $\lambda = 0.01$ and $\eta = 0.01$. (See Table 2 for values of τ)

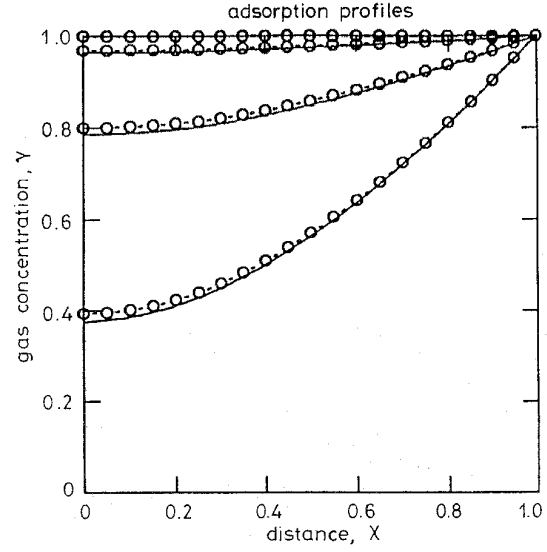

Fig. 15 *Case IV adsorption profiles for gas concentration*

The solid lines show the numerical solution and the symbols show the approximate analytical solution with $\kappa = 10^{-4}$, $\lambda = 100$ and $\eta = 0.01$. (See Table 2 for values of τ)

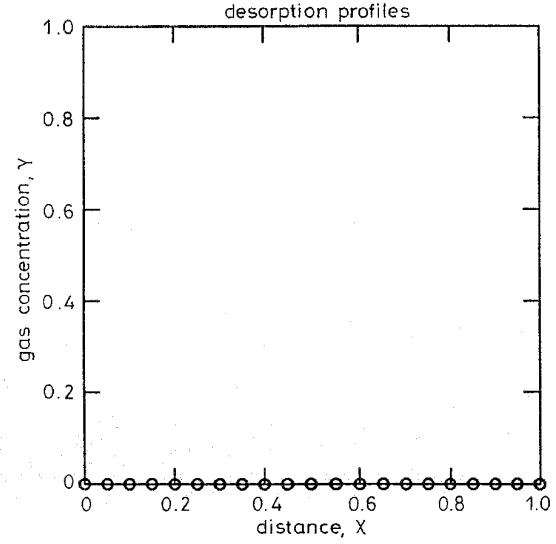

Fig. 16 *Case IV desorption profiles for gas concentration*

The solid lines show the numerical solution and the symbols show the approximate analytical solution with $\kappa = 10^{-4}$, $\lambda = 100$ and $\eta = 0.01$. (See Table 2 for values of τ)

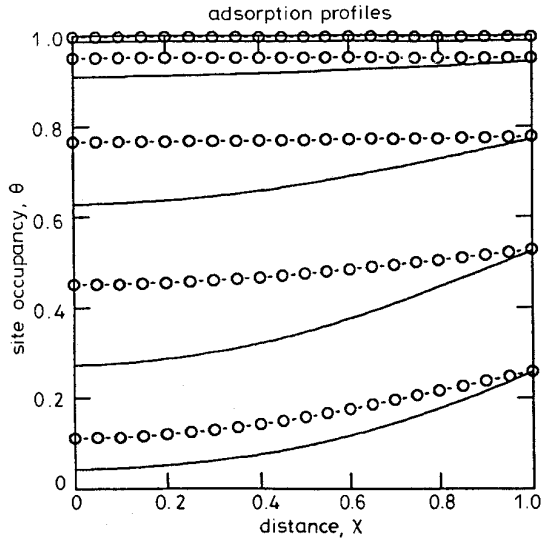

Fig. 17 *Case IV adsorption profiles for site occupancy*

The solid lines show the numerical solution and the symbols show the approximate analytical solution with $\kappa = 10^{-4}$, $\lambda = 100$ and $\eta = 0.01$. (See Table 2 for values of τ)

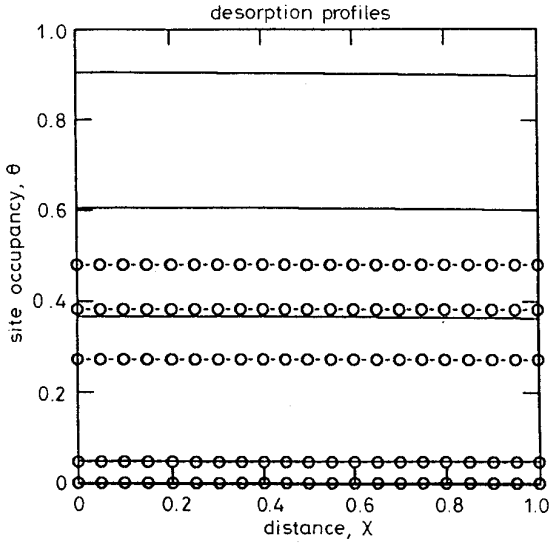

Fig. 18 *Case IV desorption profiles for site occupancy*

The solid lines show the numerical solution and the symbols show the approximate analytical solution with $\kappa = 10^{-4}$, $\lambda = 100$ and $\eta = 0.01$. (See Table 2 for values of τ)

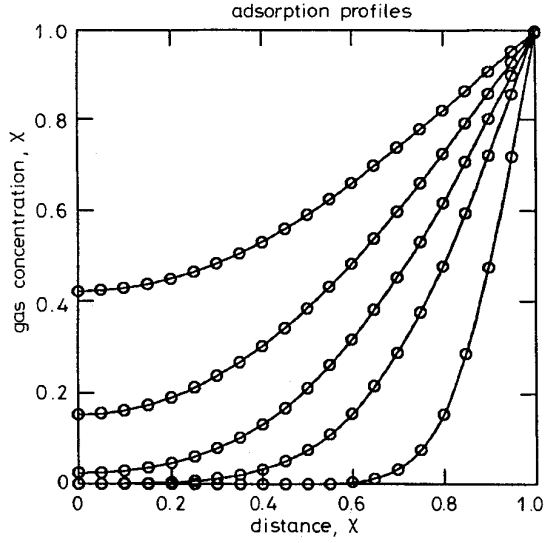

Fig. 19 *Case V adsorption profiles for gas concentration*

The solid lines show the numerical solution and the symbols show the approximate analytical solution with $\kappa = 1$, $\lambda = 100$ and $\eta = 0.01$. (See Table 2 for values of τ)

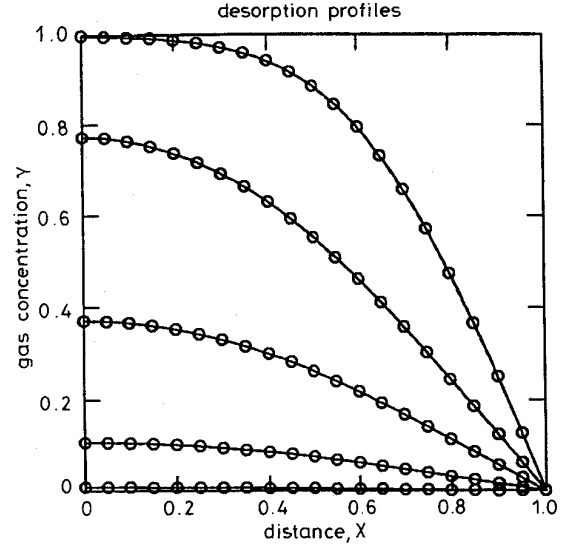

Fig. 20 *Case V desorption profiles for gas concentration*

The solid lines show the numerical solution and the symbols show the approximate analytical solution with $\kappa = 1$, $\lambda = 100$ and $\eta = 0.01$. (See Table 2 for values of τ)

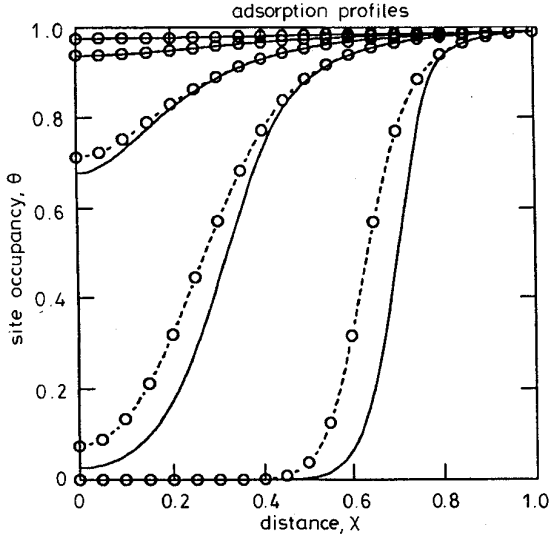

Fig. 21 *Case V adsorption profiles for site occupancy*

The solid lines show the numerical solution and the symbols show the approximate analytical solution with $\kappa = 1$, $\lambda = 100$ and $\eta = 0.01$. (See Table 2 for values of τ)

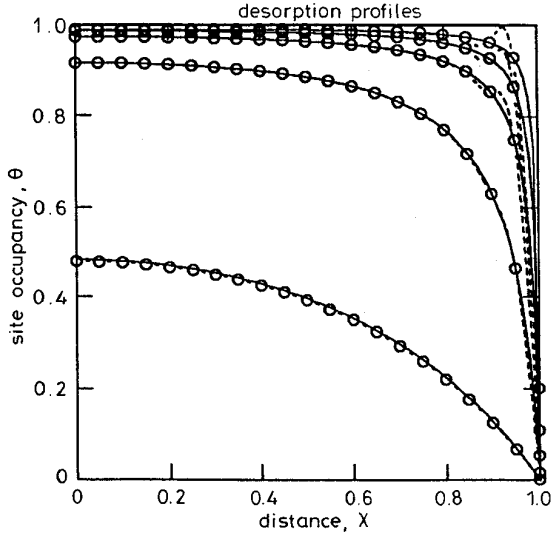

Fig. 22 *Case V desorption profiles for site occupancy*

The solid lines show the numerical solution and the symbols show the approximate analytical solution with $\kappa = 1$, $\lambda = 100$ and $\eta = 0.01$. (See Table 2 for values of τ)

and the exact numerical solution. Not only does our model predict all possible classes of behaviour but also the accuracy of that prediction improves as the case parameters move further away from the case boundaries. This validates the use of our approximate expressions to model the characteristic behaviour of conductance in polymer devices.

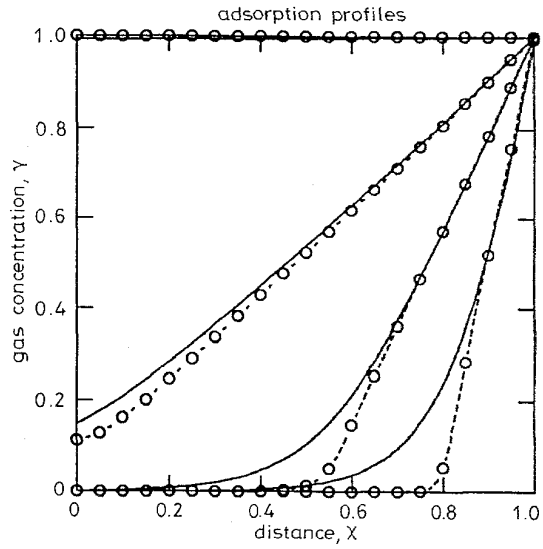

Fig. 23 *Case VI adsorption profiles for gas concentration*
The solid lines show the numerical solution and the symbols show the approximate analytical solution with $\kappa = 100$, $\lambda = 10$ and $\eta = 1{,}000$. (See Table 2 for values of τ)

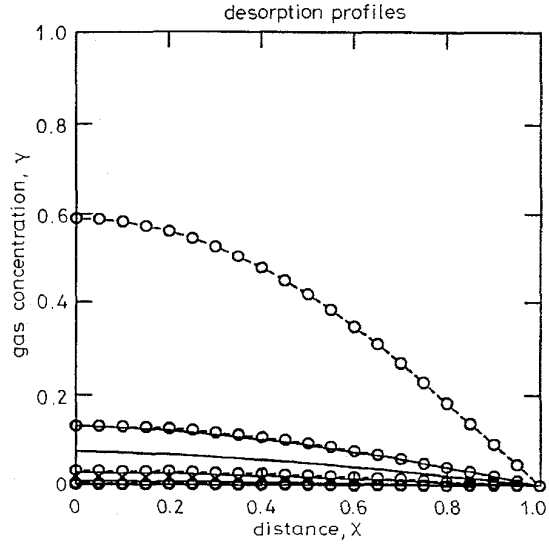

Fig. 24 *Case VI desorption profiles for gas concentration*
The solid lines show the numerical solution and the symbols show the approximate analytical solution with $\kappa = 100$, $\lambda = 10$ and $\eta = 1{,}000$. (See Table 2 for values of τ)

5 Device conductance model

The precise mechanism by which conduction takes place in conducting polymers is not well understood. It is however generally accepted that the temperature dependence of the film conductance is described by a variable range-hopping model. In the light of this we will simply consider a conducting polymer as a 3-D randomly distributed array of N identical resistive links. Each link represents a barrier to the movement of an electron within the film, i.e. to hop from one conjugated polymer backbone onto another. Then we can assume that a certain number n of these links are modified by an adsorbed gaseous molecule. Thus we have $n\theta$ links of resistance R_{filled} and $(N - n\theta)$ links of resistance R_0.

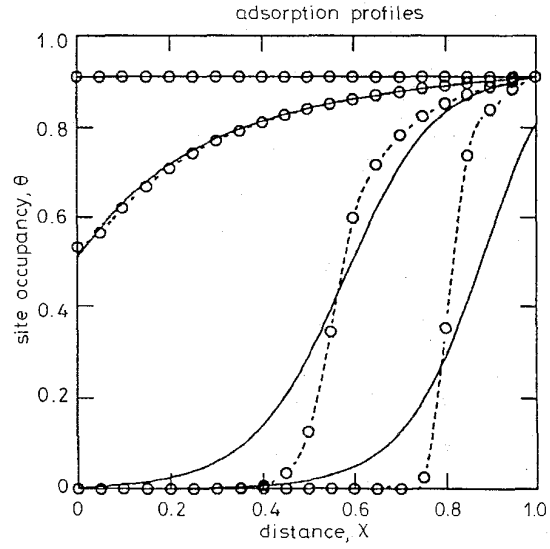

Fig. 25 *Case VI adsorption profiles for site occupancy*
The solid lines show the numerical solution and the symbols show the approximate analytical solution with $\kappa = 100$, $\lambda = 10$ and $\eta = 1{,}000$. (See Table 2 for values of τ)

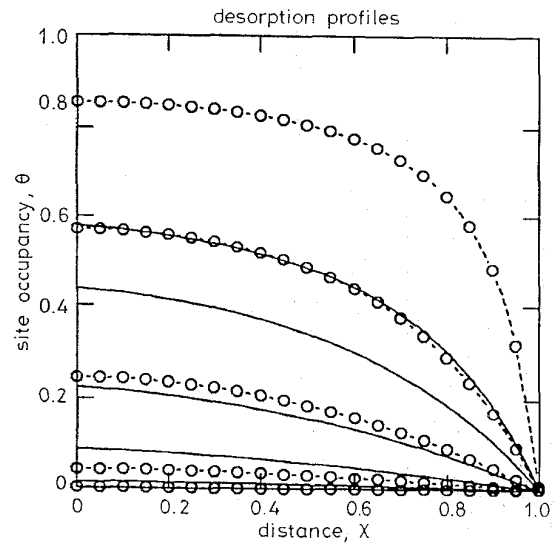

Fig. 26 *Case VI desorption profiles for site occupancy*
The solid lines show the numerical solution and the symbols show the approximate analytical solution with $\kappa = 100$, $\lambda = 10$ and $\eta = 1{,}000$. (See Table 2 for values of τ)

The macroscopic resistance (or conductance) of such a system is determined by the way in which we connect up these N resistors. For example, in a simple model, links connected in series have a total resistance proportional to the site occupancy, links connected up in parallel have a conductance proportional to the site occupancy whereas sophisticated 3-D models on disordered networks such as effective medium theory suggest that the conductance is approximately proportional to the square of the site occupancy (above the percolation threshold) [29]. Due to the complex nature of this problem and the fact that the gas effects are small, we will assume the simplest possible model in which the film conductivity $\sigma(\chi, \tau)$ is linearly

related to the site occupancy, namely

$$\sigma(\chi, \tau) = \sigma_0[1 - S\theta(\chi, \tau)] \quad (4)$$

where S is gas-sensitivity coefficient for the polymer and σ_0 is the conductivity of the film in the absence of a gas (i.e. the base-line value). This linear model does in fact describe experimental data taken on conducting polymers in which the steady-state response follows the form of a Langmuir isotherm [9]. The change in steady-state conductance is typically observed to be 1 to 10% with saturation occurring at high gas concentrations. Consequently, it seems reasonable to assume this simple model. It should be noted that the choice of the functional form relating the conductivity to the site occupancy is not constrained by our model (see below).

Fig. 27 shows two electrode geometries that are typically used in planar gas-sensitive electronic devices. The

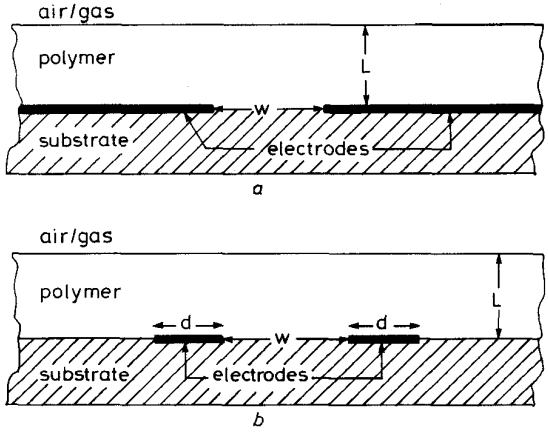

Fig. 27 *Device geometries*
a Semi-infinite electrodes
b Coplanar thin electrodes

geometry in Fig. 27*a* represents the case of a pair of semi-infinite thin electrodes with a separation of w and length b (i.e. $b \gg w$). The electric field bisecting the electrodes has been determined using Schwartz–Christoffel transformations [30] to be:

$$E_a(\chi, 0) = \frac{V}{L\pi} \Big/ \sqrt{(\chi^2 + w^2/4L^2)} \quad (5)$$

where V is the voltage applied across the electrodes (see Fig. 1). This equation assumes that there is a constant medium in the semi-infinite region above the electrodes. In fact, any differences between the relative dielectric permittivities of the substrate, polymer and air will influence the distribution of the field lines. Devices realised so far have used substrate materials with a relative dielectric permittivity similar to a conducting polymer ($\varepsilon_r \approx 8$), e.g. alumina with $\varepsilon_r \approx 10$ [14], silicon nitride with $\varepsilon_r \approx 8$ [31] and thermal oxide with $\varepsilon_r \approx 5$. As the electric field distribution within the field is integrated along a line to calculate the device conductance (see below), we believe that the sensor response is not very sensitive to this assumption. In practice, the parametric form of eqn. 5 has been verified elsewhere when a similar model was used to calculate the device conductance and applied to experimental data on poly(pyrrole). It was found that there was a good fit of steady-state conductance in air against film thickness [18], which suggests that our assumption about the electric field provides a reasonable functional form. An exact solution requires a numerical solution to the problem, e.g. by a finite-element analysis of the device layout.

The current i passing between the electrodes can now be calculated by integrating the product of the local conductivity and the electric field over a closed surface [25, 29]. Thus the conductance in air G_0 can be calculated from the geometry as

$$G_0 = \frac{\sigma_0 b}{\pi} \ln\left[\frac{1 + \sqrt{(1 + w^2/4L^2)}}{w/2L}\right]$$

(semi-infinite electrodes) (6)

Rearranging eqn. 4 (corrected version of eqn. 8 in Ref. 24.) and putting the terms in the surface integral gives the response of the device (i.e. fractional change in conductance) as

$$\frac{G(\tau) - G_0}{G_0} = \frac{\sigma(\tau) - \sigma_0}{\sigma_0} = -S \frac{\int_0^1 \theta(\chi, \tau)/\sqrt{(\chi^2 + w^2/4L^2)}\, d\chi}{\ln[1 + \sqrt{(1 + w^2/4L^2)}/[w/2L]]} \quad (7)$$

Note that in this equation changing our assumptions for the functional form of the conductivity can be accommodated by replacing $\theta(\chi, \tau)$ within the numerator of the integral in the numerator by another functional form. Similarly, we can define the sensor response as the fractional change in resistance when desirable for other sensor materials.

The steady-state response of the device can now be related to the external gas concentration a_∞ by,

$$\frac{G(\tau = \infty) - G_0}{G_0} = -S\theta_\infty = -S \frac{Ka_\infty}{[1 + Ka_\infty]} \quad (8)$$

The magnitude and size of the steady-state response depends upon the sensitivity coefficient S and hence the gas detected but not on the device geometry. Typical responses lie in the range of 1 to 10% for organic solvents. Poly(pyrrole) devices generally show a conductance which falls (i.e. $S > 0$) on the introduction of a gas [10], however the sign seems to depend upon the hydrophobicity of the polymer/counter ion system.

The second electrode geometry shown in Fig. 27*b* is a pair of *finite* coplanar thin electrodes of width d for which the conformal transformation is a Jacobean elliptical integral of the first kind giving the electric field as:

$$E_b(\chi, 0) = \frac{V}{2A^*L^2} \frac{1}{\sqrt{([\chi^2 + w^2/4L^2][M^2\chi^2 + w^2/4L^2])}} \quad (9)$$

where M is a geometrical modulus ($w/(w + 2d)$) and the constant A^* is determined from the complete elliptical integral, i.e.

$$A^* = \frac{2}{w} \int_0^1 \frac{dt^*}{\sqrt{([1 - t^{*2}][1 - M^2t^{*2}])}} \quad (10)$$

Again the effect of any dielectric behaviour of the film could be taken into account by the effective lowering of the electric field by a simple factor. Similarly the sensor's response can be calculated for this coplanar electrode structure as:

$$\frac{G(\tau) - G_0}{G_0} = -S \frac{\int_0^1 \theta(\chi, \tau)\, d\chi/\sqrt{([\chi^2 + w^2/4L^2][M^2\chi^2 + w^2/4L^2])}}{\int_0^1 d\chi/\sqrt{([\chi^2 + w^2/4L^2][M^2\chi^2 + w^2/4L^2])}} \quad (11)$$

where the steady-state response is still given by eqn. 8 but the base-line conductance G_0 becomes,

$$G_0 = \frac{\sigma_0 b}{2A^* L} \int_0^1 d\chi / \sqrt{([\chi^2 + w^2/4L^2][M^2\chi^2 + w^2/4L^2])}$$

(coplanar electrodes) (12)

So eqns. 7 and 11 give the theoretical dynamic response, and eqn 8 the steady-state response, of two planar polymer gas devices in terms of the site occupancy profiles for each of the six limiting cases discussed above.

In calculating the conductances of these devices we have assumed that the electrode thickness is much less than the film thickness and that the electrodes are long (i.e. $b \gg w$ and $b \gg d$) so that edge effects become insignificant. In principle, the model could be extended to include both these effects but in practice this is not usually necessary. Moreover, the use of an interdigitated array of electrodes could be approximated to a pair of coplanar electrodes ($w < L$) or the electric field recalculated with the appropriate boundary conditions. Finally, the model assumes that the polymer film behaves as a 3-dimensional homogeneous structure. Provided that the conjugation length in the film has a typical size much less than the electrode gap, then this assumption is valid. If not then it is possible to extend the model to take account of percolation paths across the electrodes by modifying the equation for the device conductance. However a more serious situation occurs when the film is anisotropic so that the homogeneous diffusion and conduction equations are no longer valid. Under these conditions it may be possible to modify the diffusion reaction equations and find analytical solutions but it is more likely that only a numerical solution to the problem is practical.

6 Analytical and numerical responses of polymeric gas sensors

Table 3 provides the values of the electrode parameters used to calculate the theoretical dynamic responses of the polymer device structures shown in Fig. 27. The values are expressed in terms of a constant film thickness, L, because the dimensionless time parameters scale with film thickness in diffusion rate dependent cases (e.g., Cases I, II and VI). For semi-infinite coplanar electrodes A & B, the values have been chosen to represent the extreme situations where either the electrode separation is wide compared with the film thickness ($w/L = 10$) and so the electric field bisecting the electrodes is practically independent of the position within the polymer (i.e. equation 5 reduces to $2V/\pi w$ when $w/L \gg \chi$), or where the electrode separation is small ($w/L = 0.1$) so that the electric field is close to zero at the outside of the polymer. These values can then be used to probe the effect of electrode geometry upon the transient response of the device.

Figs. 28 to 39 show the response of the polymer devices (defined by eqn. 7) for all six cases when gas is first adsorbed and then desorbed by the film. The responses are calculated using the values of parameters given in Tables 2 and 3 with the gas-sensitivity coefficient S set to 1 for convenience; this means that the steady-state response is simply $-\theta_\infty$ (from eqn. 8). The lines indicate the numerical solutions and the symbols

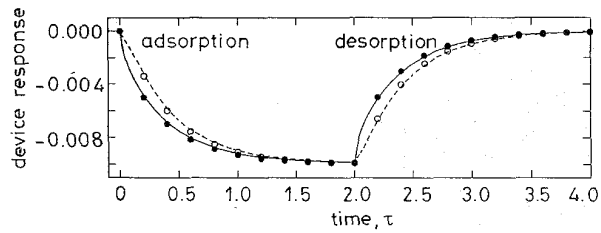

Fig. 28 *Theoretical responses of polymer devices for Case I with semi-infinite electrodes*

The lines show the numerical solutions and the symbols show the approximate analytical solution using the values taken from Tables 2 and 3. The solid line and filled symbols are for $w/L = 10$, and the dotted line and unfilled symbols are for $w/L = 0.1$

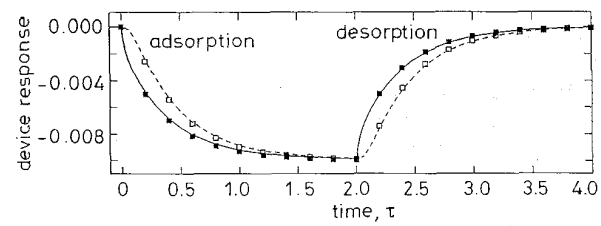

Fig. 29 *Theoretical responses of polymer devices for Case I with finite electrodes*

The lines show the numerical solutions and the symbols show the approximate analytical solution using the values taken from Tables 2 and 3. The solid line and filled symbols are for $w/L = 10$, and the dotted line and unfilled symbols are for $w/L = 0.1$

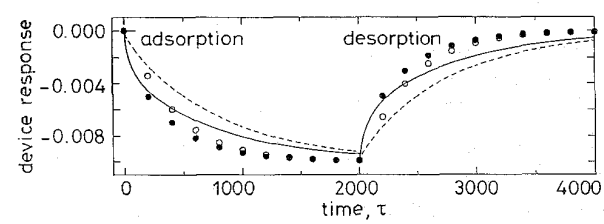

Fig. 30 *Theoretical responses of polymer devices for Case II with semi-infinite electrodes*

The lines show the numerical solutions and the symbols show the approximate analytical solution using the values taken from Tables 2 and 3. The solid line and filled symbols are for $w/L = 10$, and the dotted line and unfilled symbols are for $w/L = 0.1$

Table 3: Geometrical device parameters used to calculate the theoretical response of gas-sensitive polymer devices at constant film thickness

Device structure	Electrode separation‡ (w)	Electrode width‡ (d)	Film thickness‡ (L)	Geometric ratio (w/L)	Geometric modulus $w/(w+2d)$	Comments
Semi-infinite A	10	N/A	1	10	N/A	Behaves as film with electric field nearly constant within the polymer
Semi-infinite A	0.1	N/A	1	0.1	N/A	Behaves as film with the electric field close to zero outside the film
Finite A	10	1	1	10	0.833	Behaves as film with dipole-like field which is nearly constant within the polymer
Finite B	0.1	0.01	1	0.1	0.833	Behaves as film with dipole-like field close to zero outside the film

‡ Values are expressed in units of film thickness.

plot the approximate analytical solutions. For finite electrodes A and B, the values of the geometrical parameters have been chosen to probe the extremes of a dipole-like electric field by keeping ratio of the electrode width d to electrode separation w small but constant (i.e. 0.1).

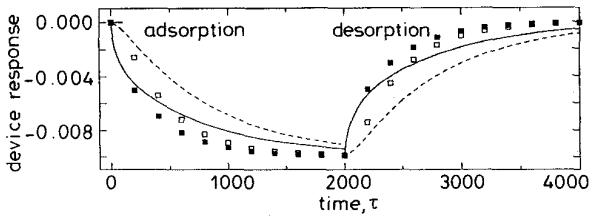

Fig. 31 *Theoretical responses of polymer devices for Case II with finite electrodes*

The lines show the numerical solutions and the symbols show the approximate analytical solution using the values taken from Tables 2 and 3. The solid line and filled symbols are for $w/L = 10$, and the dotted line and unfilled symbols are for $w/L = 0.1$

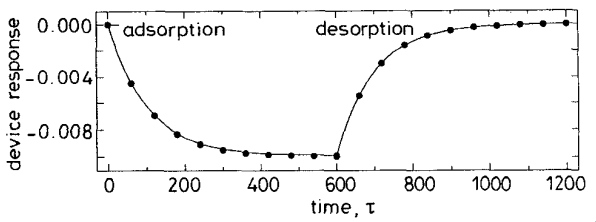

Fig. 32 *Theoretical responses of polymer devices for Case III with semi-infinite electrodes*

The lines show the numerical solutions and the symbols show the approximate analytical solution using the values taken from Tables 2 and 3. The solid line and filled symbols are for $w/L = 10$, and the dotted line and unfilled symbols are for $w/L = 0.1$ but are overlaid by an exact fit

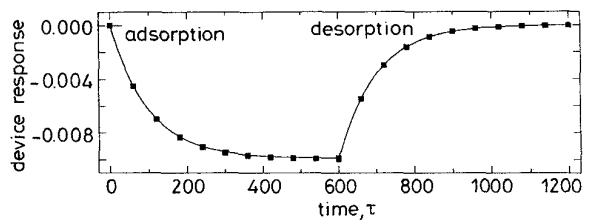

Fig. 33 *Theoretical responses of polymer devices for Case III with finite electrodes*

The lines show the numerical solutions and the symbols show the approximate analytical solution using the values taken from Tables 2 and 3. The solid line and filled symbols are for $w/L = 10$, and the dotted line and unfilled symbols are for $w/L = 0.1$ but are overlaid by an exact fit

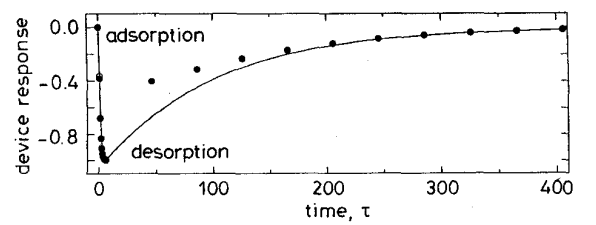

Fig. 34 *Theoretical responses of polymer devices for Case IV with semi-infinite electrodes*

The lines show the numerical solutions and the symbols show the approximate analytical solution using the values taken from Tables 2 and 3. The solid line and filled symbols are for $w/L = 10$, and the dotted line and unfilled symbols are for $w/L = 0.1$ but are overlaid by an exact fit

Figs. 28 and 29 shows the results for Case I in which the process is dominated by the diffusion of the gas into and out of the film. The adsorption and desorption profiles are symmetrical, as one would expect, and the fit of the analytical solution is exact. At constant film thickness, the profiles are slightly different with the wider electrode separation (solid lines and filled symbols) giving a shorter rise and fall time. Of course if the electrode separation was held constant and the film thickness was increased then the real time constants would scale in pro-

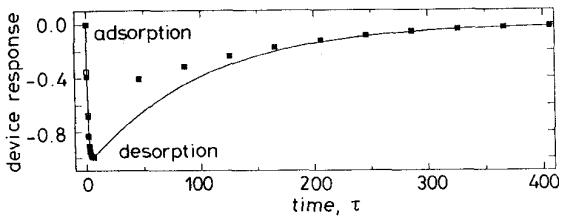

Fig. 35 *Theoretical responses of polymer devices for Case IV with finite electrodes*

The lines show the numerical solutions and the symbols show the approximate analytical solution using the values taken from Tables 2 and 3. The solid line and filled symbols are for $w/L = 10$, and the dotted line and unfilled symbols are for $w/L = 0.1$ but are overlaid by an exact fit

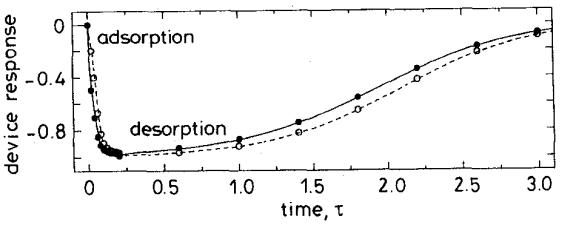

Fig. 36 *Theoretical responses of polymer devices for Case V with semi-infinite electrodes*

The lines show the numerical solutions and the symbols show the approximate analytical solution using the values taken from Tables 2 and 3. The solid line and filled symbols are for $w/L = 10$, and the dotted line and unfilled symbols are for $w/L = 0.1$

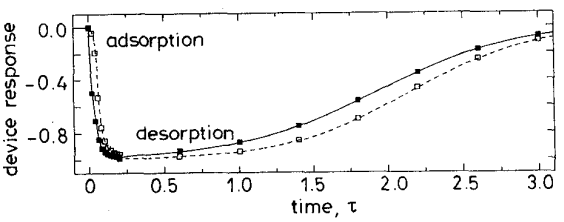

Fig. 37 *Theoretical responses of polymer devices for Case V with finite electrodes*

The lines show the numerical solutions and the symbols show the approximate analytical solution using the values taken from Tables 2 and 3. The solid line and filled symbols are for $w/L = 10$, and the dotted line and unfilled symbols are for $w/L = 0.1$

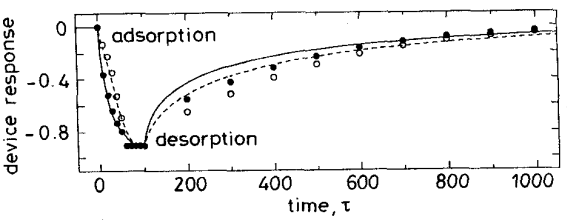

Fig. 38 *Theoretical responses of polymer devices for Case VI with semi-infinite electrodes*

The lines show the numerical solutions and the symbols show the approximate analytical solution using the values taken from Tables 2 and 3. The solid line and filled symbols are for $w/L = 10$, and the dotted line and unfilled symbols are for $w/L = 0.1$

portion to L^2. Case II (Figs. 30 and 31) is similar in that the profiles are diffusion rate limited but now there are a significant number of sites to adsorb the gas. This slows down the diffusion process as can be seen by the much larger values of τ. The analytical solutions slightly under-

estimate the rise and fall times of the process. Figs. 32 and 33 show the completely different Case III in which the behaviour is limited by the reaction kinetics of the adsorption process. Thus, the profiles are both symmetrical and independent of the electrode geometry. The rise and fall times are independent of the film thickness L and

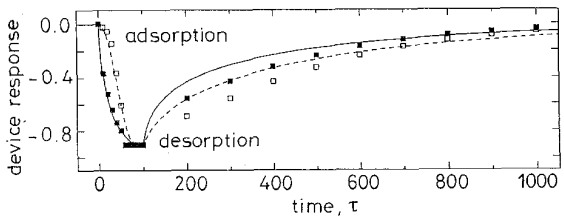

Fig. 39 *Theoretical responses of polymer devices for Case VI with finite electrodes*

The lines show the numerical solutions and the symbols show the approximate analytical solution using the values taken from Tables 2 and 3. The solid line and filled symbols are for $w/L = 10$, and the dotted line and unfilled symbols are for $w/L = 0.1$

are determined solely by the reaction rates. Case IV (Figs. 34 and 35) is also reaction rate limited but in this case there is a high concentration of gas and only a few sites. Consequently, the sites are quickly filled but upon desorption a considerable time elapses before sufficient of the large amount of gas leaves the polymer to reduce the site occupancy. As seen from the figure, the effect of the electrode configuration is small and the fit to the desorption process is less good at short times. In Case V (Figs. 36 and 37), the analytical fit is excellent with the fall time once again being much longer than the rise time but now a dependence on electrode geometry is observed. In this case the sorption sites are not saturated and so the nonlinear part of the isotherm is reached. This seems to generate a point of inflexion in the responses that has not been seen in Cases I to IV. Finally, Case VI (Figs. 38 and 39) shows the response of the polymer device when the process is neither diffusion rate nor reaction rate limited, i.e. the moving boundary problem. A very sharp adsorption profile is observed as the moving front reaches the electrodes with the narrow electrode separation. However, the desorption profiles of the different electrode geometries are similar and slow so there is no great advantage obtained from selecting the narrow-gapped device.

7 Conclusions

A conductance model of gas-sensitive conducting polymer devices has been developed in which approximate analytical expressions have been found for six limiting cases. Theoretical device responses have been computed for all six cases which show reasonable agreement with numerical solutions of the exact equations. The transient response observed in each case is either independent of the electrode structure or weakly dependent upon it at constant film thickness. Reaction rate limited cases (e.g. III) may be separated from diffusion rate limited cases (e.g. I and II) as the time constants of the former are independent of the film thickness but depend upon the external gas concentration. Cases IV, V and VI are distinguished by their desorption process being slower than that of adsorption. The choice of electrode geometry, i.e. semi-infinite versus finite coplanar, appears relatively unimportant; however the choice of a thin film is preferable in diffusion-rate limited cases.

The choice of large electrode separation to film thickness ratio is preferable in the cases where diffusion plays a role (i.e. cases I, II, V and VI). However, it has been observed that some polymers swell when they adsorb a gas in which case the design of the electrode geometry is critical. For example, if one wants to remove the effect of swelling in the device response, then a large electrode separation to film thickness ratio should be chosen. In contrast, a small electrode separation to film thickness ratio will include the effect. In which case, as the polymer swells the current is integrated over a greater electric field volume and so the device response (i.e. fall in conductance) will be enhanced (this assumes that the film conductivity is only weakly dependent upon the swelling process). For linear sensors in which the conductance rise is proportional to concentration, it may be possible to balance out the two effects of a change in electric field and a change in the charge mobility on swelling and thus design a device insensitive to a specific gas. This behaviour has been recently observed in some polymeric capacitive devices.

The model ignores any dielectric effect of the polymer upon the distribution of the field lines within a coplanar capacitor. This is not a concern unless the dielectric permittivity of the film is more sensitive to the gas or vapour concentration than its electrical conductivity, i.e. when the film is both a good dielectric and its dielectric permittivity greatly differs from that of the gas or vapour being detected. In this case the field distribution would vary with gas concentration and influence the device conductance.

In conclusion, a parametric model has been developed for gas-sensitive polymer devices that identifies six different types of behaviour or characteristic response. This model may be used to help in the rational design of new polymer devices and interpret experimental data.

8 Acknowledgment

J.W. Gardner wishes to thank the Alexandar von Humboldt Foundation for their generous financial support of his research fellowship in Germany during part of which this paper was written.

9 References

1 NYLANDER, C., ARMGRATH, M., and LUNDSTRÖM, I.: 'An ammonia detector based on a conducting polymer', *Anal. Chem. Symp. Series*, 1983, **17**, pp. 203–207
2 MIASIK, J.J., HOOPER, A., and TOFIELD, B.C.: 'Conducting polymer gas sensors'. J. Chem. Soc., Faraday Trans. 1, 1986, **82**, pp. 1117–1126
3 BLANC, J.P., DEROUICHE, N., EL HADRI A., GERMAIN, J.P., MALEYSSON, C., and ROBERT, H.: 'Study of the action of gases on a polypyrrole film'. Sensors and Actuators B, 1990, **1**, pp. 130–133
4 HANAWA, T., KUWABATA, S., and YONEYAMA, H.: 'Gas sensitivity of polypyrrole films to NO_2'. J. Chem. Soc., Faraday Trans. 1, 1988, **84**, pp. 1587–1592
5 JOSOWICZ, M., and JANATA, J.: 'Suspended gate field-effect transistor modified with polypyrrole as alcohol sensor'. Anal. Chem., 1986, **58**, pp. 514–517
6 JOSOWICZ, M., and JANATA, J.: 'Suspended gate field-effect transistors', *in* SEIYAMA, J. (Ed.): 'Chemical sensor technology, Vol 1' (Elsevier, 1988), pp. 153–177
7 CASSIDY, J., FOLEY, J., PONS, S., and JANATA, J.: 'Polymer coatings on suspended metal mesh field effect transistors', *Anal. Chem. Symp. Series*, 1986, **25**, pp. 309–314
8 JOSOWICZ, M., JANATA, J., ASHLEY, K., and PONS, S.: 'Electrochemical and ultraviolet spectrochemical investigation of selectivity of potentiometric gas sensors based on polypyrrole'. Anal. Chem., 1987, **59**, pp. 253–258

9 BARTLETT, P.N., and LING-CHUNG, S.K.: 'Conducting polymer gas sensors. Part II: response of polypyrrole to methanol vapour'. Sensors and Actuators, 1989, **19,** pp. 141–150
10 BARTLETT, P.N., and LING-CHUNG, S.K.: 'Conducting polymer gas sensors. Part III: results for four different polymers and five different vapours'. Sensors and Actuators, 1989, **20,** pp. 287–292
11 PERSAUD, K.C., and PELOSI, P.: 'Gas sensors: towards an artificial nose', *in* DARIO, P. (Ed.): 'Sensors and sensory systems for advanced robots'. NATO ASI Series F Vol. 43 (Springer-Verlag, 1988), pp. 361–381
12 PERSAUD, K.C., and PELOSI, P.: 'Sensor arrays using conducting polymers for an artificial nose', *in* GARDNER, J.W., and BARTLETT, P.N. (Eds.): 'Sensors and sensory systems for an electronic nose' (Kluwer Academic Press, *1991*), pp. 237–256
13 BARTLETT, P.N., and GARDNER, J.W.: 'Odour sensors for an electronic nose', *in* GARDNER, J.W., and BARTLETT, P.N. (Eds.): 'Sensors and sensory systems for an electronic nose' (Kluwer Academic Press, 1991), pp. 31–51
14 PEARCE, T.C., GARDNER, J.W., FRIEL, S., BARTLETT, P.N., and BLAIR, N.: 'An electronic nose for monitoring the flavour of beers'. Analyst, 1993, **118,** pp. 371–377
15 DIAZ, A.F., RUBINSTEIN, J.F., and MARK, H.B.: 'Electrochemistry and electrode applications of electroactive conductive polymers', *in* 'Advances in polymer science, Vol. 84' (Springer, 1988), pp. 113–139
16 DIAZ, A.F., and BARGON, J.: 'Electrochemical synthesis of conducting polymers', *in* 'Handbook of conducting polymers, Vol. 1' (Dekker, 1986), pp. 81–115
17 HEINZE, J.: 'Electrically conducting polymers', *in* 'Topics in current chemistry, Vol. 152' (Springer, 1990), pp. 1–47
18 BARTLETT, P.N., ARCHER, P., and LING-CHUNG, S.K.: 'Conducting polymer gas sensors. Part I, fabrication and characterisation'. Sensors and Actuators, 1989, **19,** pp. 125–140
19 BLACKWOOD, D., and JOSOWICZ, M.: 'Work function and spectroscopic studies of interactions between conducting polymers and organic vapours'. J. Phys. Chem., 1991, **95,** pp. 493–502
20 JOSOWICZ, M., and TOPART, P.: 'Studies of the interactions between organic vapours and organic semiconductors: applications to chemical sensing', *in* GARDNER, J.W., and BARTLETT, P.N. (Eds.): 'Sensors and sensory systems for an electronic nose' (Kluwer Academic Press, 1991), pp. 117–129
21 TOPART, P., and JOSOWICZ, M.: 'Characterisation of the interaction between poly(pyrrole) films and methanol vapour'. J. Phys. Chem., 1992, **96,** pp. 7824–7830
22 SLATER, J.M., WATT, E.J., FREEMAN, N.J., MAY, I.P., and WEIR, D.: 'Gas and vapour detection with polypyrrole gas sensors'. Analyst, 1992, **117,** pp. 1265–1270
23 BARTLETT, P.N., and GARDNER, J.W.: 'Diffusion and binding of molecules to sites within homogeneous thin films'. Trans. Roy. Soc., *1995 (at press)*
24 GARDNER, J.W., and BARTLETT, P.N.: 'Design of conducting polymer gas sensors: modelling and experiment'. Synthetic Metals, 1993, **55–57,** pp. 3665–3670
25 GARDNER, J.W.: 'A diffusion-reaction model of electrical conduction in tin oxide gas sensors'. Semicond. Sci. Technol., 1989, **4,** pp. 345–350
26 CRANK, J.: 'Mathematics of diffusion' (Oxford Univ. Press 1975), p. 286
27 BRITZ, D.: 'Digital simulation in electrochemistry', 2nd ed. (Springer-Verlag, 1988)
28 CRANK, J., and NICOLSON, P.: 'A practical method for numerical evaluation of solutions of partial differential equations of the heat-conduction type'. Proc. Cambridge Phil. Soc., 1947, **43,** pp. 50–67
29 CUSSACK, N.E.: 'The physics of structurally disordered matter' (Adam Hilger 1987), p. 235
30 GARDNER, J.W.: 'Electrical conduction in solid-state gas sensors'. Sensors and Actuators, 1989, **18,** pp. 373–387
31 GARDNER, J.W., PIKE, A., DE ROOIJ, N.F., KOUDELKA-HEP, M., CLERC, P.A., HIERLEMANN, A., and GOEPEL, W.: 'Integrated array sensor for detecting organic solvents'. Sensors and Actuators B, 1995, **26–27,** pp. 135–139